IJARCCE

ISSN (Online) 2278-1021
ISSN (Print) 2319 5940

International Journal of Advanced Research in Computer and Communication Engineering
Vol. 5, Issue 1, January 2016

Selection Process for Area Identification of Articular Cartilage

Prof. Dr. S. L. Lahudkar[1], Chetana Kurve[2]

Electronics and Telecommunication, JSPM's Imperial College of Engineering and Research, Pune, India [1]

Abstract: In biomedical science so many process have come to cure the malfunction of human body in any manner without any suppression. This enhancement of medical therapy gives the new ray to every issues related to medical such as dialysis, any transplantation in body, asthama, blood issues, etc. In this fastest and growing age of life a new and common disease has come named as osteoarthritis which means a disease which is caused due to lack of fluid in the joints of bones. For this there are a lot of programmed therapy and a lot of medicines are available, but to cure it for long there are some parameters introduced named as processing, segmentation, ray images, etc. All this are needful because we need a good and effective output in short time. So, here in this area the procedure of selection for process for this joint can be done on the basis of that we will conclude which one is effective and best.

Keywords: knee joint, segmentation process, MR images.

I. INTRODUCTION

The human body consists of hard and soft tissues connected with each other and helps in the body function. One of the important connections in the body was made by ligaments which connects bones to each other at joints functions. It is present in the end of the bones through which the bones can slide against each other in a proper manner giving easy movement also provide a stable connection and strength. The extensive joint as compared to others is knee joint which provides the ease of moving from one place to another, with the ability of bearing the hole body weight, balance it and enables the frictionless movement in joints. Cartilage a tissue which is a fluid material covers the knee joint and provides flexible movement.

The continuous movement in the joints leads to the degradation in the slippery material causes an anabiometric disease called as Osteoarthritis (OA). It is a clinical syndrome of the joint pain. The main symptoms are pain and stiffness in the joint at motions and even a crakle sound produced due to the rubbing of bones over each other at joints. This disease mainly occurred in 75% of peoples includes old age and adults.
The ends of articulating bones in diarthrodial joints are covered by a thin (1 mm to 6 mm), dense connective tissue called articular cartilage. In the knee joint, articular cartilage covers the patella, tibia and femur, mainly in the regions where these bones come in contact to one another. The patellar cartilage is the thickest (3.0 mm on average) and the tibial is the thinnest (1.6 mm on average). More study of the knee joint can be extracted from the textbook Basic Biomechanics of the Musculoskeletal System.

II. LITERATURE REVIEW

OA is caused by an abnormal wearing of cartilage that situated on all sides of joints, which performs as a spring mounted material and decreases friction in the joints. In result, the area of the bone around the degenerated cartilage is more loaded than it would be under usual conditions. The missing cartilage is sometimes exchanged by bone matter. In the last stage of degeneration the bone surface begins to rub. Due to the reduce in the bones results in pain, connective and non connective t issues covering in the affected joint may become lax, results in the disability causes movement.
As various segmentation algorithms are present for analysis of different images based on their needs. These methods provide easy and simplest way to operate the object at their levels. Some are manually operated, some gives output but for accurate and color complexity it needs manual operations whereas some are self operated gives the accurate results. On the basis of the interventions these methods are introduced for different approach.

However, semi-automatic segmentation tools were also developed mainly in the project. The main motto behind this was the collaboration with the Biomechanics lab, Switzerland for characterization of changes in patellar cartilage during long span of immobilization. For this study, improvement of speed and segmentation accuracy was required. This collaboration resulted in the Ph.D. thesis of Benedicte Vanwanseele.
To enhance the area to expertise the process as informed will get selected so that on the basis of their terms we can apply for the treatment. To get the best result it is important to know the working of the process very well. So here are the terms as b spline, M REP based segmentation processes. For all this process the automatized cartilage segmentation is necessary because in this the images can the treated on the basis of 3D images only.

A. B spline: A method for segmentation was implemented as part of the main application ("ACS"). In order to segment a certain anatomical structure, the user must delineate its boundary using a B-spline curve on each slice in the data volume that contains the structure. The shape of the B-spline curve is defined interactively, by moving its control points with the mouse in the image slice. The user

DOI 10.17148/IJARCCE.2016.51104

IJARCCE

ISSN (Online) 2278-1021
ISSN (Print) 2319 5940

International Journal of Advanced Research in Computer and Communication Engineering
Vol. 5, Issue 1, January 2016

has the possibility to add new control points or remove existing ones. An algorithm similar to was implemented for fine adjustment of the spline's control-points, based on the image information. However, this algorithm was not applied automatically for each spline curve; instead, the user could choose whether or not to run it at any stage of the segmentation process. A description of the adjustment algorithm is given below. The position of each control point was estimated by performing the following steps for each control point of the current "B-spline":

1. Compute the 2D gradients over a one-dimensional profile with radius R, centered in the current control point, along the direction of the normal n to the curve in that point:

$$gi = g(pi) = Ґ(I(pi)), i = -\overline{R, R} \quad (1)$$

In the above equation, Ґ(I(pi)) represents the gradient operator at position pi in the 3D image I. As already specified, the positions pi were situated along the normal n of the current atom and their values were calculated as:

$$pi = o + i \cdot \sigma n, i = -\overline{R, R} \quad (2)$$

where o is the position of the atom's node; σ is the step size and controls, on one hand, the accuracy of the fit and on the other, together with the radius R, the size of the search space.

2. From the resulting 2D gradient profile G = {g(−R), . . . , g0, . . . , gR}, the scalar gradient profile ˜G = {g(−R), . . . , g0, . . . , gR} along the direction given by the atom's normal was calculated by projecting each element on n:

$$gi = g(pi) \cdot n, i = -\overline{R, R} \quad (3)$$

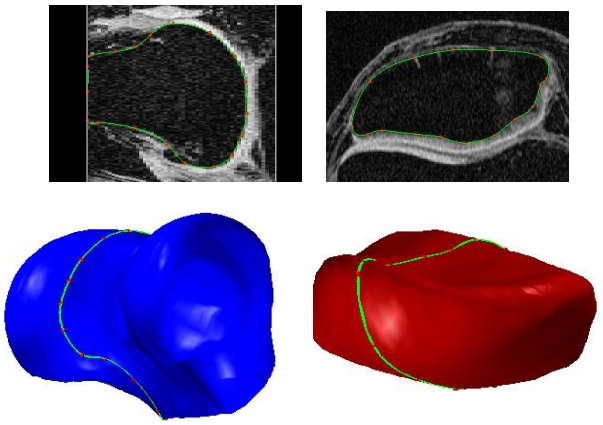

Figure 1: Example of "B-spline" segmentation of the femur (a), and the patella (b) bones. The upper row depicts how the B-spline contour delineates the object of interest on a slice from an MR volume. On the lower row, the reconstructed surfaces meshes are shown, with the spline contours from the upper row highlighted on the surface.

3. The node was moved to the position pi that corresponded to the highest gradient in the vector ˜G. It should be noted that in the algorithm presented above, the orientation of the normal was changed to always points towards the interior of the spline curve. Otherwise, the scalar gradients' values would be all negated and the smallest gradient would indicate the position of the cartilage boundary.

B. M-REP-based segmentation : In the last subsection, a method was introduced that uses a boundary representation (B-REP) of the object of interest, where the object's boundary was represented by a stack of 2D "B-spline" curves. Such a representation can, in principle, be used for processing of any kind of object. However, when manual processing is involved, some specialized techniques can be used in order to increase the ease of interaction to the model One class of techniques, which is well suited for manipulating sheet-like objects, uses a medial model to represent the two- or three-dimensional objects. The medial representation (M-REP) was first introduced and is based on the ideas of medial axis descended. Unlike the medial axis, an M-REP is a multi-scale approach that uses a natural (width-proportional) sampling of the medial surface, in place of a continuous manifold. At each of the sampling points on the medial axis, a medial atom is placed that implies two opposing sections on the object's boundary. As illustrated, a medial atom m consists of

• A position x ∈ R3, i.e. the skeletal position;
• A radius r ∈ R+, that gives the distance from the skeletal position to the implied boundary positions;
• A coordinate frame F =(n, b, b⊥) implying the tangent plane to the skeleton (via its normal n) and the particular unit vector in that tangent plane that is along the direction of the fastest narrowing/widening between the implied boundary sections (b);
• An object angle $\theta \in \left[0, \frac{\pi}{2}\right]$ that determines the angulation of the implied section of boundary relative to b.

The two opposite boundary points processed by the medial atom with position x are given by y1 = x + p and y2 = x + s. The vectors p and s are defined as:

$$p = rR(b,n)(\theta)b$$
$$s = rR(b,n)(-\theta)b \quad (4)$$

where R(b,n)(θ) is a rotation by θ in the (b, n) plane.

Depending on its shape, a 3D object can then be represented by a net or sequence of medial atoms. In the following, we shall refer only to nets of medial atoms, as they are the representation of choice for articular cartilage. Nevertheless, the same techniques can be applied for sequences of medial atoms, which are mainly used for representing tube-like objects.
From the sparse quadrilateral meshes of medial atoms, a continuous medial surface is defined via B´ezier interpolation of the discretely sampled medial atoms. In similar fashion, the surface of the object is also interpolated as a bicubic scalar field on the interpolated medial manifold, given the atoms' radia r. In the original version of, the atoms may have any position and orientation in the 3D space. However, manipulation of the atoms in 3D is still a difficult task, especially when high accuracy is required. On the left column, one row of the

DOI 10.17148/IJARCCE.2016.51104

IJARCCE

ISSN (Online) 2278-1021
ISSN (Print) 2319 5940

International Journal of Advanced Research in Computer and Communication Engineering
Vol. 5, Issue 1, January 2016

M-REP mesh is depicted, while on the right column, the surface mesh implied by the M-REP is shown for each of the two cartilages.

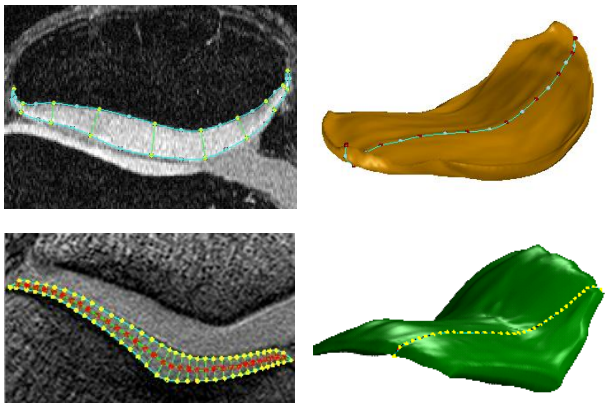

Figure 2: Example of M-REP segmentation of the patellar (upper row) and femoral cartilage.

The M-REP rows from the left column are also highlighted on the surfaces on the right application of the semi-automatic segmentation for articular cartilage; external restrictions were imposed to the medial atoms. According to these restrictions, each row of atoms from the quadrilateral mesh could only be placed on a transversal slice from the 3D MR volume. Also, the coordinate frame was redefined as F' = (n, b), where the atom's normal n is given by:

$$n = \frac{y2-y1}{|y2-y1|} = \frac{s-p}{|s-p|} \qquad (5)$$

and the unit vector b was obtained by a 90 rotation of n in the transversal slice plane

$$b = R_{\perp}\left(\frac{\pi}{2}\right) n \qquad (6)$$

III.DESIGN

Other approaches exist in which only the middle spline is initialized manually and then automatically adjusted to match the image information. The adjusted spline curve is then propagated on the neighbouring slices and used as initial position for the same automatic adjustment algorithm. Such a method was not implemented in this work, as the assumptions made about the variation of the objects' contour between adjacent slices make the method less generic. However, the user had the possibility to copy an existing curve to an unprocessed slice and then run the adjustment process on it. The B-spline segmentation delivers sub-voxel precision, since the control points can be moved at a finer scale in the scaled-up image (performed using OpenGL zooming). Additionally, the image can be smoothed with a linear filter available from the OpenGL library and its corresponding gradient. Once the whole object is segmented, the corresponding set of 2D spline curves must be converted to a 3D triangular mesh. In the general case, when the object contains holes and branches, this problem is far from trivial, since direct conversion requires additional information about the object's topology. This post-processing operation has been studied extensively and proved to be a difficult problem that cannot be solved in an unique way.

One poble workaround is to use an indirect technique that first converts the stack of contours into a 3D binary volume. After that, the triangular mesh is obtained using any of the methods from the previous subsection. It seems as this method would suffer from the same problem regarding the precision as the voxel based approach, i.e. its precision being limited to the size of a voxel in the data volume. However, this is not the case, since the binary volume can be created using arbitrarily small voxel size. Also, the implicit smoothing of the B-spline curves helps in reducing the plateau-effect. If, on the other hand, the object is of simple topology, without branching, a direct surfacing method can be applied for obtaining the mesh representation. This was also true in our case, as the segmentation was restricted to one curve per slice, so the inter-curve connections could be defined in a straightforward manner. The following paragraphs describe the direct method for converting a set of spline curves into a 3D closed surface. The algorithm uses only local information from adjacent curves, therefore it will be detailed only for two spline curves S(i) and S(i+1), situated on consecutive image slices.

The above modifications allowed for direct manipulation of the atom's boundary points y1 and y2 in the 2D space of the transversal image slice. Segmentation of the articular cartilage was performed using a multi-resolution approach, starting with a coarse medial grid and adjusting its parameters according to the image information. For the adjustment of the boundary points, the method described in previous subsection was employed. After all atoms were adjusted, the medial grid was refined either by adding new rows or columns and the same optimization process was performed on the newly inserted atoms.

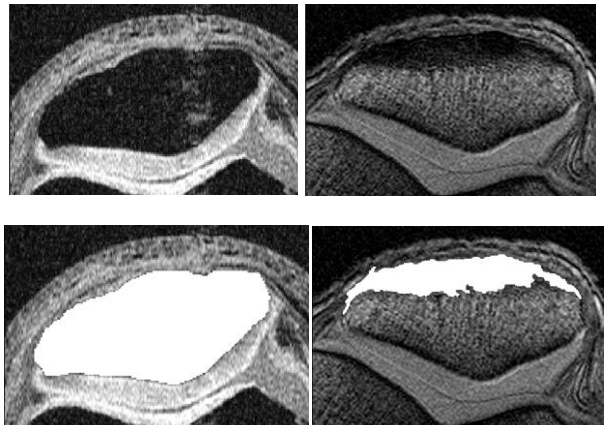

(a) (b)

Figure 3: Two results of the voxel-based segmentation of the patellar bone. (a) The bone originated from a fat-suppressed scanning protocol is homogeneous, therefore it was well segmented. The algorithm could handle the blood-flow artefact running through the right side of the bone. (b) In a water selective protocol the bone has significantly large bright regions, thus the voxel-based segmentation fails.

DOI 10.17148/IJARCCE.2016.51104

In some cases, at the end of the adjustment process, the resulting medial representation must be transformed to a triangular surface mesh. This process is much simpler than the one described in the previous subsection, due to the inherent ordering of the quadrilateral mesh that holds the M-REP. Hence, each quadrilater can be approximated by uniformly sampling it on its two directions and then triangles can be generated by splitting the resulting rectangles over one of their diagonals.

IV. CONCLUSION

In this design of the process we can conclude that if we are going to segment the image in articular cartilage ligament the effects of the fluid will get easily extracted, as also the 3D representation of the images is also going to get processed. On the basis of this 3D image the functioning of the cartilage ligament can be processed with the help of above modifications on the terms identified. The segmentation is performed with a coarse medical grid with its parameters which can get adjusted later also by editing some optimization processes.

ACKNOWLEDGMENT

I are rather infused by the kind guidance of **Dr. S. L. Lahudkar** who put me in cradle of our engineering studies and evaluated us to this end mean of my dissertation, without his guidance, I am sure to be an orphan in the vast ocean of the subject. Ultimately no tongue could describe the deep sense of cooperation and ready nature to help us in minute the details of my write up of this topic. It was his constant, tireless guidance and constructive criticism that made me to move on and i am also thankful to my production house Michael Shell for developing and providing chance to present my thoughts which have been used in this template.

REFERENCES

1. L. P. Clarke, R. P. Velthuizen, M. A. Camacho, J. J. Heine, M. Vaidyanathan, L. O. Hall, R. W. Thatcher, and M. L. Silbiger, "MRI segmentation: methods and applications," Magn. Reson. Imag., vol. 13, no. 3, pp. 343-368, 1995.
2. Gao, B., Zheng, N., 2009. Alterations in three-dimensional joint kinematics of anterior cruciate ligament-deficient and – reconstructed knees during walking. Clinical Biomechanics 25: 222–229.
3. Beynnon, B., Johnson, R., Fleming, B.C., Kannus, P., Kaplan, M., Samani, J., Renstro¨m, P., 2002. Anterior cruciate ligament replacement: comparison of bone-patellar tendon-bone graft with twostrand hamstring grafts. J. Bone Joint Surg. 84-A: 1503–1513.
4. Peña, E., Calvo, B., Martínez, M.A., Doblaré, M., 2006. Influence of the tunnel angle in ACL reconstructions on the biomechanics of the knee joint. Clinical Biomechanics 21: 508–516.
5. Rathnayaka, K., Momot, K.I., Noser, H., Volp, A., Schuetz, M. A., Sahama, T., Schmutz, B., 2012. Quantification of the accuracy of MRI generated 3D models of long bones compared to CT generated 3D models. Medical Engineering & Physics 34: 357-363.
6. Hao, Z., Jin, D., Zhang, Y., Zhang, J., 2007. A finite element 3D model of in vivo human knee joint based on MRI for the tibiofemoral joint contact analysis. Digital Human Modeling, HCII 2007, LNCS 4561: 616-622.

DOI 10.17148/IJARCCE.2016.51104